A Model Structure of the Muscle Protein Complex $4Ca^{2+}$·Troponin C·Troponin I Derived from Small-Angle Scattering Data: Implications for Regulation†

Glenn A. Olah and Jill Trewhella*

Chemical Science and Technology Division, Los Alamos National Laboratory, Los Alamos, New Mexico 87545

Received June 14, 1994; Revised Manuscript Received August 17, 1994®

ABSTRACT: We report here a model structure for $4Ca^{2+}$·troponin C·troponin I derived from small-angle X-ray and neutron scattering data using a Monte Carlo modeling method. In this model, troponin I appears as a spiral structure that wraps around $4Ca^{2+}$·troponin C which adopts an extended dumbbell conformation similar to that observed in the crystal structures of troponin C. The troponin I spiral has the approximate dimensions of an α-helix and winds through the hydrophobic "cups" in each globular domain of troponin C. The model is consistent with a body of previously published biochemical data on the interactions between troponin C and troponin I, and suggests the molecular mechanism for the Ca^{2+}-sensitive switch that regulates the muscle contraction/relaxation cycle involves a signal transmitted via the central spiral region of troponin I.

In the sliding filament model of muscle contraction, interdigitating thick and thin filaments move past each other, resulting in contraction and relaxation. The thick filaments are composed of myosin, while the thin filaments are made from a helical assembly of actin monomers with tropomyosin polymerized head to tail in the grooves of the actin helix, and each tropomyosin bound to one troponin. The contractile force is thought to be generated when the myosin heads, S1, cyclically attach and detach from specific sites on the actin monomers, whereby a power stroke, driven by actin–S1–myosin ATPase activity, occurs sometime during the attachment phase of the cycle. Troponin and tropomyosin form a Ca^{2+}-sensitive switch which regulates the interactions between myosin and actin [reviewed by Leavis and Gergely (1984) and Zot and Potter (1987)]. Troponin has three subunits: troponin C (TnC)[1] which binds Ca^{2+}, troponin I (TnI) which inhibits the actin–S1–myosin ATPase activity, and troponin T (TnT) which binds troponin to tropomyosin. The X-ray crystal structures of TnC (Herzberg & James, 1985; Sundaralingam et al., 1985) show a dumbbell-shaped molecule, with C- and N-terminal globular domains connected by an extended 8–9-turn solvent-exposed α-helix. The C-terminal domain contains two high-affinity Ca^{2+}/Mg^{2+} binding sites (sites III and IV), thought to always be occupied in muscle, while the N-terminal domain contains two low-affinity Ca^{2+}-specific sites (sites I and II) (Potter & Gergely, 1975), which are not occupied in the crystal structure. Comparison of the structurally similar N- and C-terminal domains indicates the effect of Ca^{2+} binding is to open the "cup"-shaped domain, exposing hydrophobic residues lining the inner surface of the cup (Herzberg et al., 1986). Interactions with these hydrophobic cup regions are thought to be important in the Ca^{2+}-dependent regulatory function. It is Ca^{2+} binding to the two low-affinity sites in the N-terminal domain of TnC which regulates the contractile event by altering the interaction of TnI with actin and releasing the inhibition of myosin attachment to actin. The TnI sequence segment 96–115 is implicated in the regulatory function and is believed to alternately bind to actin or to $4Ca^{2+}$·TnC (Syska et al., 1976; Talbot & Hodges, 1981).

Recently we completed small-angle X-ray and neutron scattering experiments on $4Ca^{2+}$·TnC·TnI and obtained new structural information on the complex in solution. These experiments are reported elsewhere in detail (Olah et al., 1994), but briefly the neutron experiment capitalized on the different neutron scattering properties of hydrogen and deuterium by measuring the scattering from a complex of deuterated $4Ca^{2+}$·TnC and nondeuterated TnI dissolved in solvents with different D_2O:H_2O ratios. We extracted from this "contrast series" the small-angle scattering profiles for each component of the complex. These profiles, combined with structural parameters also determined from the scattering data such as the radius of gyration, R_g, the maximum linear dimension, d_{max}, the separation of the centers-of-mass of the components, the symmetry of the components, and the relative dispositions of symmetry axes, provide a set of constraints that severely limit the possible models for the complex. While the one-dimensional data obtained from small-angle solution scattering experiments are in general not sufficiently constraining to uniquely define a three-dimensional structure, in the case of the $4Ca^{2+}$·TnC·TnI complex the combination of constraints from the scattering data, the previously determined crystal structure of TnC, and known molecular volumes allowed a low-resolution structure to be derived. The nucleosome core particle had a similar set of structural constraints which facilitated the successful modeling of its solution structure using small-angle scattering data, thus revealing the nucleosome protein core surrounded by double-helical DNA in a helical superstructure (Pardon et al., 1975, 1977; Hjelm et al., 1977). This structure was subsequently confirmed by X-ray crystallography experiments (Finch et al., 1977).

† This work was performed under the auspices of the Department of Energy (Contract W-7405-ENG-36) and supported in part by an appointment of G.A.O. to the Alexander Hollaender Distinguished Postdoctoral Fellowship Program sponsored by DOE/Office of Health and Environmental Research, and administered by the Oak Ridge Institute for Science and Education. It was also supported by National Institutes of Health Grant GM40528 (J.T.) and DOE/OHER Project KP-04-01-00-0 (J.T.). The neutron data used for this study were obtained using facilities at the Manuel Lujan Jr. Neutron Scattering Center, a national user facility funded by DOE/Office of Basic Energy Sciences, and facilities at the National Institute of Standards Technology, U.S. Department of Commerce, supported by the National Science Foundation under Agreement DMR-9122444.

® Abstract published in *Advance ACS Abstracts,* October 1, 1994.

[1] Abbrevations: d_{max}, maximum linear dimension; MLCK, myosin light chain kinase; R_g, radius of gyration; R_c, radius of gyration of cross section; TnC, troponin C; TnI, troponin I; TnT, troponin T.

0006-2960/94/0433-12800$04.50/0

To model the structure of $4Ca^{2+}$·TnC·TnI, we developed a Monte Carlo method that allowed us to rapidly evaluate possible models for the complex against the scattering data. This method has allowed an exhaustive search of possible models consistent with the starting model constraints. We present here a description of the modeling approach, the results of the model search and refinement, a comparison of the final model with published biochemical data, and a brief discussion of the implications of the model for regulation. Since high-resolution structural data on the $4Ca^{2+}$·TnC·TnI complex are not currently available, the low-resolution model derived from the scattering data will serve as an important guide for experiments aimed at further delineating the structure/function relationship for this key Ca^{2+}-sensitive molecular switch.

MATERIALS AND METHODS

Starting Model Parameters. Table 1 summarizes the structural parameters derived from the X-ray/neutron scattering experiments, while Figure 1 shows the derived scattering profiles [$I(Q)$ vs $\mathbf{Q}$; $\mathbf{Q}$ is the scattering vector defined as $(4\pi \sin \theta)/\lambda$, where θ is half the scattering angle and λ is the wavelength of the incident radiation] for the overall complex and its individual components (Olah et al., 1994). The inverse Fourier transform of the experimental scattering profiles (Moore, 1980) gives the respective vector length or pair distribution functions, $P(r)$ (Figure 2). $P(r)$ is the frequency of interatomic vector lengths within the molecular boundary and goes to zero at the maximum linear dimension, d_{max}. The second moment of $P(r)$ gives the radius of gyration, R_g, for the scattering particle. The $P(r)$ profiles for each component and for the complex indicate highly asymmetric, elongated structures. A comparison of the $P(r)$ profiles for TnC calculated from the crystal structure and from the neutron experiment shows them to be very similar (Figure 2B). Both profiles show the characteristic peak at ≈18 Å corresponding to the most probable vector length within the individual globular domains, a secondary peak at ≈45 Å corresponding to the most probable interdomain vector length, and a d_{max} of 72 Å. We therefore concluded the structure of $4Ca^{2+}$·TnC in the complex is similar to the crystal structure in that the helix connecting the two globular domains fully extended. The $P(r)$ profile for TnI indicates an even more asymmetric structure than TnC. The multiple peaks (at 43 and 86 Å) and shoulder (at 10–20 Å) preclude a simple uniform rod shape (which would give a single peak due to the diameter of the rod and steadily decrease with increasing vector length), but rather indicate a structure with repeating features or domains.

Guinier analysis of the very low-$\mathbf{Q}$ scattering data gives average radius of gyration of cross section, R_c, values for each component and the complex (Table 1) that indicate their long axes are all approximately coincident (Olah et al., 1994). The variation of R_g with neutron scattering for the complex indicates the separations of their centers-of-mass are also approximately coincident (<10 Å) and the higher scattering density component (deuterated $4Ca^{2+}$·TnC) is more toward the inside of the complex than the lower scattering density component (TnI) (Olah et al., 1994). Additionally, the TnI component is significantly more extended than the TnC, with a d_{max} equal to that of the entire complex.

The scattering data thus constrain the possible models for the complex to structures in which the TnC component is in an extended configuration, similar to the crystal structure, with TnI encompassing and extending beyond TnC, approximately symmetrically, at both ends of the long axis of the complex. We estimate the "dry" volume of TnI to be ≈26 000 Å^3 based on its molecular weight and an assumed partial specific volume of 0.74 cm^3/g (Wilkinson & Grand, 1975, 1978). The hydrated volume is expected to be ≈46% larger than this value (Chen & Bendedouch, 1986). A cylindrical structure encompassing TnC would thus have much too large a volume. The 43 Å periodicity and prominent 10–20 Å structural feature in the TnI $P(r)$ function, combined with the d_{max} value, indicate TnI forms some sort of regular spiral-like structure that winds from one end of TnC to the other, extending approximately 20 Å beyond TnC at each end. Such a structure would give rise to multiple peaks in the $P(r)$ distribution arising from the diameter of the spiral, and the periodicity of its path. The volume constraint on TnI and the dimensions of TnC restrict the number of possible turns of the spiral structure to approximately two or less, while the d_{max} of ≈118 Å restricts the product of its pitch and number of turns.

Table 1: Comparison of Structural Parameters Derived from Scattering Data[a] and the Final "Best Fit" Model

		R_g (Å)	R_c (Å)	d_{max} (Å)
$4Ca^{2+}$·TnC	experiment	23.9 ± 0.5	10.7 ± 1.0	72 ± 3
	model	24.1	10.3	73
TnI	experiment	41.2 ± 2.0	20.5 ± 2.0	118 ± 4
	model	40.1	20.5	114
$4Ca^{2+}$·TnC·TnI	experiment	33.0 ± 0.5	16.2 ± 1.5	115 ± 4
	model	33.4	15.7	117

Separation (Å) of the Centers-of-Mass of $4Ca^{2+}$·TnC and TnI	
experiment	<10[b]
model	4.2
Angle (Degrees) between Long Axes of $4Ca^{2+}$·TnC and TnI	
experiment	0[c]
model	6.4

[a] Experimental parameters from Olah et al. (1994). [b] From analysis of the contrast dependence of R_g (Olah et al., 1994). [c] From analysis of R_c values (Olah et al., 1994).

Monte Carlo Modeling Method. A Monte Carlo method was used to construct and test models for TnI and the $4Ca^{2+}$·TnC·TnI complex. The Monte Carlo approach has been used by us before to evaluate models against scattering data (Heidorn & Trewhella, 1988; Olah et al., 1993), but this application required developing the software to rapidly test models while independently varying all the structural parameters defining the structural classes. The Monte Carlo method involves defining the molecular boundaries of a model structure and placing that structure within a box. Random points are generated within the box, and those points which fall within the molecular boundary are saved. Distances between every pair of saved points representing that model are determined. The maximum length of the model is divided up into approximately 200 channels each of fixed width into which the pair distances are binned. The resulting histogram is the calculated $P(r)$ function for the model. Model intensity profiles for comparison with the experimental profiles are readily calculated from the $P(r)$ functions by a Fourier inversion (Moore, 1980; Olah et al., 1993). Minimum reduced-χ^2 values comparing the model and experimental scattering profiles for both the complex and the TnI component were used as "best fit" criteria. Each model structure tested required approximately 1 min for calculations using a 486 IBM/PC (50 MHz).

Since a high-resolution structure of the TnC component is available, it was modeled using homogeneous spheres representing each amino acid positioned at each α-carbon crystal-

lographic coordinate. The sizes of the spheres are determined from the volumes of each amino acid. In addition, a 1 Å layer was placed around the molecule to simulate bound water. Since the TnC structure was not varied during the initial model search, the random points representing it only had to be generated once and saved. TnI model structures were generated as uniform density shapes constrained to have a molecular volume within a factor of 2 of the "dry" protein volume, and random points were generated within each geometric shape to be tested. The number of random points in the TnC and TnI components was proportional to their respective scattering densities multiplied by their volumes. The number of random points representing TnI was set at 700, sufficient to guarantee statistical variations are negligible. With the number of random points for TnI fixed, the appropriate number of random points representing $4Ca^{2+}$·TnC can be determined for representation of the total complex.

In order to test models of the complex, the components had to be positioned with respect to each other. Since the scattering data constrain the long axes of the two components and their centers-of-mass to be approximately coincident, the long axis of the interconnecting helix of the TnC was initially fixed along the z-axis, coincident with the TnI long axis. Later, better fits to the measured data were found when the center-of-masses of the N- and C-domains of TnC were placed on the z-axis. This latter orientation of TnC also resulted in better contact with TnI and minimal overlap between the two components.

RESULTS

The TnI structure can be divided into three regions: a central region that interacts with the length of the TnC and two end regions that can interact primarily with the outer edges of the N- and C-terminal lobes of the TnC. Initially, a number of classes of models were systematically tested against the scattering data. The models tested consisted of a central spiral structure with between 0.5 and 2 turns capped with different geometric shapes. At the resolution of the scattering data, the possible shapes for the cap regions can be approximated by semiellipsoids, cylinders, or toroids. Model searches in which the parameters defining the central spiral region and the two cap regions represented by semiellipsoids or cylinders were completed by systematically incrementing the structural parameters defining those shapes over the range of possible values consistent with the molecular volume. Models with semiellipsoids or cylinders could not reasonably fit the scattering data for TnI and $4Ca^{2+}$·TnC·TnI simultaneously. For example, using semiellipsoid caps, the "best fit" to TnI resulted in a reduced-χ^2 value of $\approx$4, but $4Ca^{2+}$·TnC·TnI had a reduced-χ^2 value of $\approx$50. Inversely, the "best fit" to $4Ca^{2+}$·TnC·TnI was $\approx$8 while that for TnI was $\approx$400. Only models with toroidal caps reasonably fit the TnI and $4Ca^{2+}$·TnC·TnI scattering data simultaneously and met the volume and d_{max} constraints. The model search described below was therefore confined to TnI models consisting of a central helical spiral capped at each end by an additional turn collapsed to zero pitch (i.e., a toroidal cap at each end).

The pitch (P), number of turns (N), minor radius (R_{min}), and major radius (R_{max}) of the central helical spiral constitute four parameters to be determined from the model refinement. The minor radius defines the thickness of the structure forming the spiral, and the major radius defines the distance of that structure from the spiral axis. The length (L) of the central spiral was initially varied between 66 and 72 Å, and the best models had this length equal to the approximate length of the TnC, i.e., $\approx$69 Å. (This was subsequently taken as a constraint, which eliminates one variable from the model search since $P = 69/N$ Å.) Two additional parameters to be varied were the minor radius (R^{cap}_{min}) and major radius (R^{cap}_{max}) of the toroidal caps. Finally, the toroidal caps do not necessarily form a complete circle, but rather some fraction of a circle giving another variable (N_{cap}). Initially, a large range with a coarse step size was chosen for each variable defining the TnI model, and all possible combinations of these variables were tested. Since the scattering data do not constrain the handedness of TnI's periodic structure, we also tested both right-handed and left-handed structures. In the model searches, reduced-χ^2 values varied considerably. The median χ^2 value was $\approx$100, with values as high as $\approx$1000 for the poorest fits and <10 for the better fits. A smaller test range and finer step size were subsequently searched about this minimum for both the left- and right-handed spiral structures. For both left- and right-handed spiral structures, one minimum was found with simultaneous reduced-χ^2 values <7 for TnI (Q-range: 0.02–0.17 Å^{-1}) and <1.6 for $4Ca^{2+}$·TnC·TnI and a volume consistent with that expected for TnI. A total of 9430 models were tested during the fine search, and only 40 met this criteria. Each of these 40 models had very similar structural parameters all falling within 10% of their mean values. The fine and coarse test ranges are tabulated in Table 2, as are the results of the "best fit" to the scattering curves for the right-handed structure (the parameters and χ^2 values for the left-handed structures were the same within error).

Since the scattering data do not distinguish the handedness of the TnI spiral, the two possibilities were evaluated against previously published biochemical and structural data on the interactions between TnC and TnI. At this stage of the refinement, the right-handed TnI structure was striking in that its central spiral path showed close interactions with the two hydrophobic cup regions in the globular domains of TnC. At the same time, it interacted closely with helices C, E, and

Table 2: Summary of Model Refinement

(A) Variables Determined in the Initial Fine and Coarse Searches, and the Respective Search Range and Increments[a]

variable	best fit value	search range	increment
N	1.0	0.7–1.2	0.1
		(0.5–2.0)	(0.5)
R_{min}	6.0	5.5–7.5	0.5
		(5.0–15.0)	(2.0)
R_{max}	13.0	12.0–16.0	0.5
		(12.0–22.0)	(2.0)
L	69	69	0
		(66.0–72.0)	(3.0)
R^{cap}_{min}	6.0	5.5–7.5	0.5
		(5.0–15.0)	(2.0)
R^{cap}_{max}	24.5	23.0–26.0	0.5
		(12.0–28.0)	(4.0)
N_{cap}	0.9	0.8–1.0	0.1
		(0.0–1.0)	(0.2)

(B) Reduced-χ^2 Values for the Best Fit Model against the Scattering Data [$I(Q)$ vs Q][b]

$4Ca^{2+}$·TnC	(i)	(ii)	Q-range (Å^{-1})
$4Ca^{2+}$·TnC	1.4	0.6	0.02–0.20
TnI	6.3	6.3	0.02–0.17
	0.9	0.9	0.02–0.15
$4Ca^{2+}$·TnC·TnI	1.1	1.0	0.02–0.20

[a] The parameters are defined in the text and are given in units of angstrom except for N and N_{cap} which are fractions of one complete turn. The values in parentheses are for the initial coarse search. [b] (i) After the fine search. (ii) After the final refinement steps involving opening the N-terminal domain of TnC and optimizing the position of TnI with respect to TnC.

G of TnC, each of which is predicted to interact with TnI [reviewed in Zot and Potter (1987)]. In contrast, the left-handed spiral could not simultaneously interact with helices C, E, and G in the TnC structure unless the structure of the TnC was altered such that the relationship between the two domains is significantly different to the crystal structure. Additionally the left-handed TnI spiral could not simultaneously interact with both hydrophobic cup regions of TnC. We therefore concluded that the left-handed structure is not correct.

The model identified at this stage of the search showed TnI shaped like a one-turn spiral, with incomplete "donut"-shaped caps at each end (i.e., the toroidal caps formed less than one full turn). The pitch of the central spiral was such that it could interact with the hydrophobic "cup" regions of each TnC globular domain, consistent with their being key points of interaction between TnC and TnI. In the crystal structure, only the high-affinity Ca^{2+} binding sites were occupied, and hence only the C-domain was in the "open" Ca^{2+}-bound configuration (Herzberg & James, 1985; Herzberg et al., 1986). In our scattering experiments, all four Ca^{2+} sites are occupied. To refine our model, we therefore modified the N-terminal domain of the crystal structure in a similar fashion to Herzberg et al. (1986) so it is more open like the Ca^{2+}-bound C-terminal domain. Specifically, we defined a hinge through the α-carbons of residues Gly_{34} and Ser_{70} and rotated the B and C helices from 0° to 64° in steps of 2°. Comparing the intensity curves calculated for each $4Ca^{2+}$·TnC model with the measured intensity curve, a distinct minimum was found in the reduced -χ^2 for a rotation of 40° [≈20° more open than the $4Ca^{2+}$·TnC model proposed by Herzberg et al. (1986); see Figure 2B and Table 2B].

A final refinement step was to optimize the position of TnC with respect to TnI by allowing the axis connecting the N- and C-domains of TnC to translate within 10 Å of and within 8° parallel to the central TnI helical axis. Optimal final positioning was guided by visual inspection of the contacts between the two components. This final refinement of the model lowered the reduced-χ^2 value for the "best fit" model to 0.6 for TnC and 1.0 for $4Ca^{2+}$·TnC·TnI (Table 2). The final "best fit" average structure had a volume of 44 000 $Å^3$ for TnI which is a reasonable value for the hydrated protein. Modeling TnI with smooth-surfaced geometric shapes might also be expected to result in an inflated molecular volume since the real protein surface will certainly be less smooth.

Figure 1 compares the scattering profiles for the complex and its components with those calculated from the final model. The agreement is excellent for the complex and for $4Ca^{2+}$·TnC. For TnI, the agreement is excellent in the Q-range 0.02–0.15 $Å^{-1}$. Above $Q = 0.17$ $Å^{-1}$, the experimental and model scattering profiles diverge. This region of the scattering profile for TnI is extremely sensitive to small errors in background subtraction because it is the weakest scattering samples that contribute most to this profile (those measured in 90 and 100% D_2O). This region is also the most affected by internal density fluctuations within the scattering particle which are not included in the TnI models. It is not surprising, therefore, that the agreement between the model and the experimental scattering profile is not good in this region. Figure 2 shows a comparison of the experimental $P(r)$ functions with model $P(r)$ functions calculated by back-transforming the model intensity profiles over the same Q-range used in the experiment. The agreement is excellent for $4Ca^{2+}$·TnC. For TnI, the model and experimental $P(r)$'s have peaks in the same places, and their relative amplitudes are similar. The model $P(r)$ has

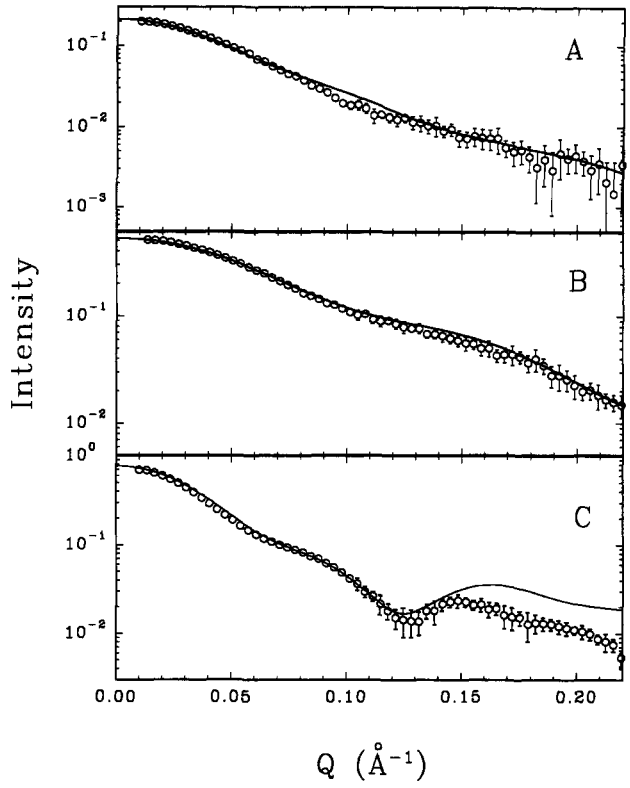

FIGURE 1: (A) X-ray scattering from $4Ca^{2+}$·TnC·TnI, uncorrected for instrument resolution or beam shape. The solid line is calculated from the model in Figure 3, with "smearing" corrections for instrument resolution and beam shape. (B and C) Scattering profiles for $4Ca^{2+}$·TnC and TnI, respectively, determined from the neutron scattering "contrast series". Analysis required these data to be corrected for instrument resolution and beam shape (Olah et al., 1994). The solid lines are the model scattering profiles calculated from the "best fit" model in Figure 3.

sharper features, however, which can be at least partly attributed to our inability to model the high-Q data for TnI (>0.15 $Å^{-1}$). For the complex, the experimental and model curves show some differences in the intensity profile in the middle vector length region. The error bars shown in the $P(r)$ profiles are propagated from the counting statistics in the scattering data and are calculated only as ±1 standard deviation. Further, they do not account for systematic errors derived, for example, from truncation effects arising from the finite Q-range measured in the experiment, or from the approximations involved in modeling TnI as a perfectly regular, smooth-surfaced structure.

The final refined structure is illustrated in Figure 3. At the resolution of our experiment, given the constraints derived from the unusual symmetries and asymmetries in this structure, we believe the basic features of this structure are uniquely defined by the scattering data. The test of this conclusion clearly lies in comparisons with independent experimental data, particularly high-resolution structural data that might now be obtainable from complexes of TnC with edited TnI molecules in which the editing can be guided by our model.

TnC/TnI Interactions. The diameter of the TnI central spiral structure is 12 Å, close to that expected for an α-helix and allowing for some effective expansion (1–2 Å) that might be expected from hydration layer effects (Chen & Bendedouch, 1986). $4Ca^{2+}$·TnC has a high affinity for peptides with sequences that have a propensity for forming basic, amphipathic α-helical structures. Small-angle scattering data from TnC complexes with short helical peptides in this class have

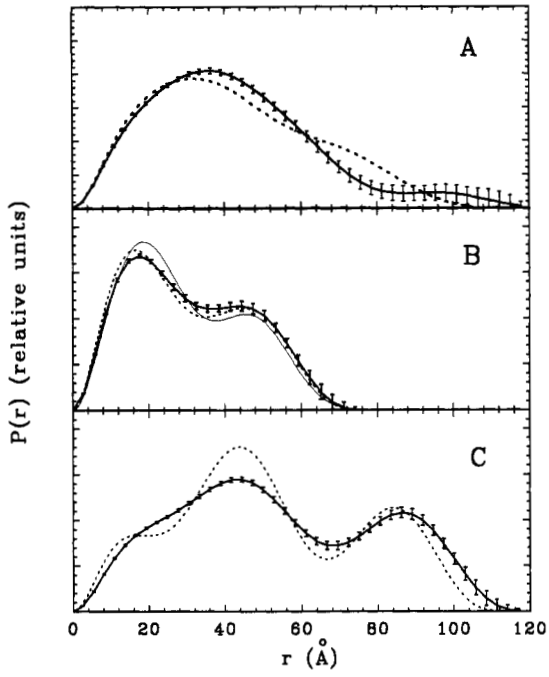

FIGURE 2: $P(r)$ functions for the $4Ca^{2+}$·TnC·TnI complex and its components corresponding to the scattering curves given in Figure 1: (A) $4Ca^{2+}$·TnC·TnI; (B) $4Ca^{2+}$·TnC; (C) TnI. The short dashed line in each panel is the model $P(r)$ function determined from the "best fit" model in Figure 3. The thin solid line in panel B is calculated from the $2Ca^{2+}$·TnC crystal structure. The error bars are propagated from counting statistics and are ±1 standard deviation.

shown TnC will sometimes, but not always, collapse around these structures such that the two globular domains of TnC come into close contact (Blechner et al., 1992). On the basis of comparisons with the structurally similar calmodulin, these basic amphipathic helices are believed to form strong interactions with the hydrophobic "cups" of the globular domains (Ikura et al., 1992; Meador et al., 1992, 1993). A Chou–Fasman analysis (Chou & Fasman, 1978) of the rabbit skeletal muscle TnI sequence (Table 3) predicts a very high proportion of α-helix, as much as 71% of the sequence. Assuming to a first approximation TnI is mostly helical, with a rise per residue of 1.5 Å, it would take ≈70–80 residues for TnI to form its spiral path from one end of TnC to the other (≈105 Å in length). The neutron data tell us the TnI mass is approximately equally distributed on either side of the TnC center-of-mass. This implies residues ≈50–130 are candidates for forming such a helical structure. Notably, this region includes the inhibitory region of TnI(96–115) proposed by a number of investigators to bind to $4Ca^{2+}$·TnC at residues 89–100 (E helix), i.e., beginning in the interconnecting helix region and extending toward the high-affinity Ca^{2+} binding site III in the C-domain (Chong & Hodges, 1981, 1982a; Grabarek et al., 1981; Dalgarno et al., 1982; Leavis & Gergely, 1984; Tao et al., 1986; Lesyk et al., 1987). Such an interaction is entirely consistent with our model. Though the Chou–Fasman calculation does not predict the inhibitory sequence segment to be α-helical, NMR data indicate it does adopt an approximately helical structure when bound to TnC (Campbell & Sykes, 1991). Altogether, the data suggest therefore that the central spiral region contains a significant amount of α-helical structure. The resolution of the structural data and the limitations of secondary structure predictions from amino acid sequence prohibit an evaluation of the exact amount of α-helix and how many other structural elements such as kinks or bends there might be.

If we have correctly placed the TnI residues in the central spiral region, then approximately residues 1–50 and 130–179 would be located in the cap regions. Thus, the TnI sequence 1–40 would be in the N-terminal TnI cap region. This sequence is believed to be a negative regulator of the TnI inhibitory region (Ngai & Hodges, 1992). It should be noted, however, that simple inspection of the "best fit" model indicates that, unlike the central spiral region, there are few intermolecular interactions to stabilize the toroidal cap regions of the structure. Since small-angle scattering only measures a time and ensemble average structure, the cap regions may be flexible in the binary complex with only an average position and orientation as shown in our model. Stabilizing contacts may have been affected by urea which was added to solutions in order to eliminate D_2O-induced aggregation (Olah et al., 1994). In the absence of urea and in the ternary troponin complex or when the binary or ternary complexes are bound to tropomyosin in the thin filament, the cap regions seem likely to have additional intermolecular contacts stabilizing their structures. Indeed, cross-linking studies have shown that TnI and TnT are closely associated (<0.6 nm) (Hitchcock, 1975) in the ternary complex and that the N-terminal region of TnI (residues 28–82) interacts with TnT (Chong & Hodges, 1982b). The N-terminal region of TnI (residues 1–98) is also necessary for incorporation of TnT into the ternary complex (Farah et al., 1994). In addition, binding of TnI to a tropomyosin affinity column has been observed; however, specific sites of interaction between TnI and tropomyosin are currently unknown (Leavis & Gergely, 1984).

Farah et al. (1994) concluded TnI and TnC are in an antiparallel orientation with respect to their N- and C-terminal domains based on studies utilizing deletion mutants of TnI and site-directed mutagenesis of TnC. Kobayashi et al. (1994) came to the same conclusion based on cross-linking studies and site-directed mutagenesis. The scattering data used here do not distinguish between an antiparallel or parallel configuration directly. However, with the TnI sequence symmetrically distributed about the TnC center-of-mass, a parallel orientation of the TnI and TnC sequences is (slightly) favored by our model for the TnI inhibitory region to interact with residues 89–100 of TnC. The resolution of the scattering data, however, is such that either orientation could be accommodated with relatively small adjustments of the precise positioning of the TnI sequence in the central spiral region (recall the centers-of-mass are coincident only to within 10 Å). A number of investigators have concluded that the TnI inhibitory sequence interacts with both the N- and C-terminal domains of TnC (Lesyk et al., 1987, 1990; Kobayashi et al., 1991). Our model appears to preclude extensive contacts between the TnI inhibitory sequence and both TnC domains. Many of the studies aimed at identifying interacting regions between TnC and TnI have involved the use of peptides, cleavage products, or edited proteins. It has been previously stated and we emphasize here that the conflicting data combined with the similarities between the N- and C-terminal domains of TnC raise concerns about the use of peptides and partial sequences to define the interactions between the intact proteins (Ngai & Hodges, 1992; Swenson & Frederickson, 1992; Olah et al., 1994). Reinforcing this concern is the observation that the TnI regulatory peptide sequence (1–40), known to bind strongly to TnC in a Ca^{2+}-dependent manner and possibly located in the N-terminal cap region of TnI, shows subtle differences when this peptide sequence binds to TnC compared with intact TnI (Ngai & Hodges, 1992).

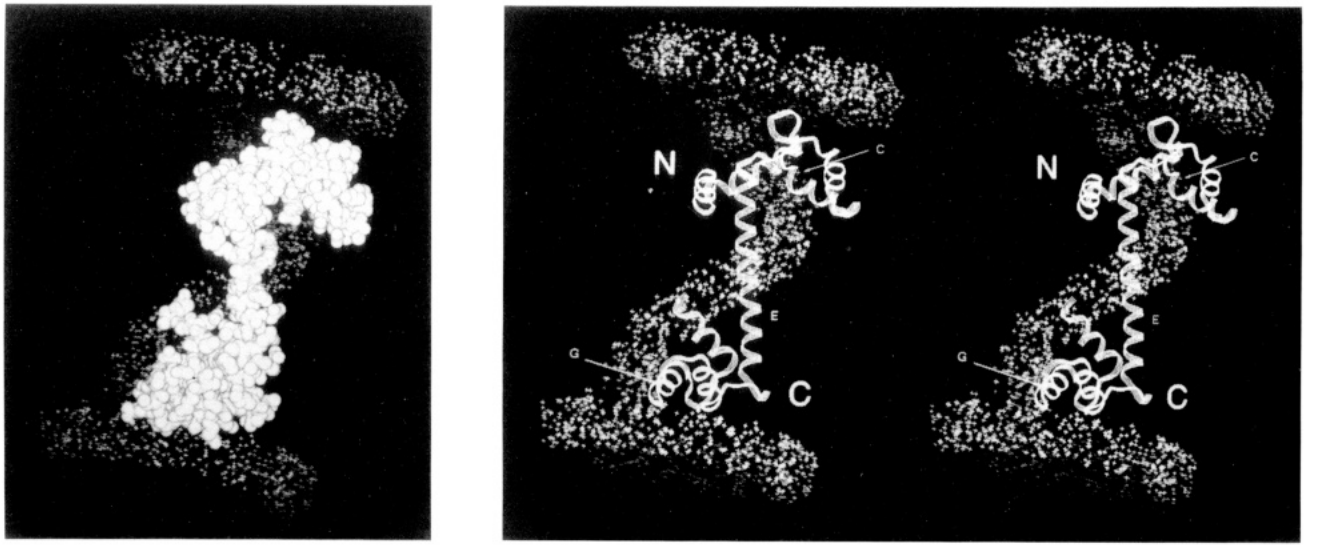

FIGURE 3: "Best fit" model for $4Ca^{2+}$·TnC·TnI. (Right) Stereoview showing the spiral path of TnI (white crosses) winding around $4Ca^{2+}$·TnC (ribbon). The N- and C-domains, as well as helices C, E, and G, of TnC are labeled. (Left) The model with $4Ca^{2+}$·TnC represented as a CPK model.

Table 3: Results of Chou–Fasman Analysis of the Rabbit Skeletal TnI Sequence[a]

```
          10        20        30        40        50        60        70        80        90
GDEEKRNRAITARRQHLKSVMLQIAATELEKEEGRREAEKQNYLAEHCPPLSLPGSMAEVQELCKQLHAKIDAAEEEKYDMEIKVQKSSK
          HHHHHHHHHHHHHHHHHHHHHHHHHHHHHHHHHHhhhHHHH          HHHHHHHHHHHHHHHHHHHHHHHHHHHHHHHHHh
           sssssssssssssssss              ssss              sssssssssssss              ssssssss
    TTTT                                  TTTT     TTTTTTTTT                                  TTTTT
CCCC     C

     **********************
          100       110       120       130       140       150       160       170
ELEDMNQKLFDLRGKFKRPPLRRVRMSADAMLKALLGSKHKVCMDLRANLKQVKKEDTEKERDVGDWRKNIEEKSGMEGRKKMFESES
hHHhhhhHHHHh              HHHHHHHHHHHHHHHhhhhHHHHHHHHHHHHHHHHHHHHH                  hHHHHHHHH
    ssssssss                    ssssss     sssssssssssss
T  TTTT     TTTT    TTTT                TTTT                      TTTTT      TTTTTTT
               CCC     C                                        C      CCCCC               C
```

[a] The letters h, s, t, and c represent helix, sheet, turn, and coil, respectively. A conformation indicated by a capital letter is more probable than one indicated by a lower case letter. The solid line indicates that region of the sequence proposed to form the central spiral structure in TnI. The asterisks designate the TnI inhibitory sequence (96–115).

DISCUSSION

Comparison with Related Structures. TnC is structurally similar to the evolutionarily related, multifunctional calcium binding protein calmodulin. The $4Ca^{2+}$·TnC·TnI model described here is distinctly different than the structures of calmodulin complexed with the short synthetic peptides based on the calmodulin binding domains in the much studied target enzymes smooth muscle and skeletal muscle myosin light chain kinase (MLCK) (Heidorn et al., 1989; Ikura et al., 1992; Meador et al., 1992, 1993). These structures show calmodulin collapses around the target peptide which folds into a short amphipathic helical structure with tight interactions with the hydrophobic "cup" regions in each globular domain of calmodulin. MLCK is typical of many calmodulin/target enzyme interactions in that calmodulin is only bound to the target in the presence of Ca^{2+}, and its binding domain is confined to a relatively short (≈20 residues) sequence segment. In contrast, like TnC in troponin, calmodulin is an integral part of the multisubunit enzyme phosphorylase kinase which has 2 noncontiguous ≈25 residue calmodulin binding subdomains (Dasgupta et al., 1989). These subdomains are contained in a 75 residue sequence segment of the catalytic subunit of phosphorylase kinase. Previous small-angle scattering experiments have shown that the structure of calmodulin when complexed with both of these subdomains has an extended structure (Trewhella et al., 1990), as does TnC complexed with the TnI inhibitory peptide (Belchner et al., 1992). Further, one of the calmodulin binding subdomains has a region of sequence identity with TnI(96–115) (Dasgupta et al., 1989). The structural and functional similarities between these systems led us to previously suggest that TnC would adopt an extended structure when bound to TnI. We would now suggest that the structure of calmodulin complexed with the 75 residue sequence segment containing the 2 calmodulin binding subdomains of the catalytic subunit of phosphorylase kinase might be very similar to the central spiral region of TnI complexed with TnC.

TnC also shows structural similarities to the regulatory and essential light chains of myosin, and these structures have recently been solved as part of the chicken skeletal muscle myosin S1 fragment (Rayment et al., 1993), and the regulatory domain of scallop myosin (Xie et al., 1994). In both these complexes, the essential and regulatory light chains abut each other while both binding to a long α-helical segment of the myosin heavy chain. The regulatory light chain is relatively extended in both structures, with a distinctive kink in the interconnecting helix region that orients the two globular lobes appropriately. Also in each case, the α-helical region of the

heavy chain twists through hydrophobic "cup" regions of the regulatory light chain globular domains in a manner similar to TnI with $4Ca^{2+}$·TnC. In contrast, the essential light chain structures are more collapsed, similar to but not as compact as calmodulin complexed with the MLCK peptides. Nature has apparently utilized these distinctive dumbbell–shaped structures with points of potential flexibility in their interconnecting helix regions to bind to a variety of helical structures of different lengths and chemical composition, for different purposes.

Implications for Regulation. Our model of the solution structure of $4Ca^{2+}$·TnC·TnI derived from the scattering data suggests a possible molecular basis for the Ca^{2+}-sensitive molecular switch that regulates the muscle contraction/relaxation cycle. In the Ca^{2+}-bound complex, both ends of the TnI central spiral region would be anchored by interactions with the open hydrophobic "cup" regions of $4Ca^{2+}$·TnC; hence, the TnI inhibitory sequence is constrained to be closely associated with $4Ca^{2+}$·TnC, and the inhibitory function of TnI is switched off. The loss of Ca^{2+} from the N-terminal low-affinity Ca^{2+} binding sites responsible for the regulation would result in a closing of that domain and release of TnI at that end, allowing enough flexibility in the central spiral region for the TnI inhibitory sequence (96–115) to shift from its binding site near the C-terminal domain of TnC to its binding site on actin, thus switching the inhibition back on. The regulatory signal would thus be transmitted via the central spiral region of TnI. Studies of mutant TnC's in which parts of the central helix region are deleted show they still interact with TnI and retain some basic function (Sheng et al., 1991; Dobrowolski et al., 1991; Babu et al., 1993). With the principal sites of interaction between TnI and TnC involving the end regions of the TnI central spiral and the TnC hydrophobic cups, it appears to be quite reasonable that the complex could accommodate deletions in the central helix region of TnC and still retain its function.

REFERENCES

Babu, A., Rao, V. G., & Gulati, J. (1993) *J. Biol. Chem. 268*, 19232.

Blechner, S. L., Olah, G. A., Strynadka, N. C. J., Hodges, R. S., & Trewhella, J. (1992) *Biochemistry 31*, 11326.

Campbell, A. P., & Sykes, B. D. (1991) *J. Mol. Biol. 222*, 405.

Chen, S.-H., & Bendedouch, D. (1986) *Methods Enzymol. 130*, 79.

Chong, P. C., & Hodges, R. S. (1981) *J. Biol. Chem. 256*, 5071.

Chong, P. C., & Hodges, R. S. (1982a) *J. Biol. Chem. 257*, 2549.

Chong, P. C., & Hodges, R. S. (1982b) *J. Biol. Chem. 257*, 11667.

Chou, P. Y., & Fasman, G. D. (1978) *Adv. Enzymol. Relat. Areas Mol. Biol. 47*, 45.

Dalgarno, D. C., Grand, R. J. A., Levine, B. A., Moir, A. J. G., Scott, G. M. M., & Perry, S. V. (1982) *FEBS Lett. 150* 54.

Dasgupta, M., Honeycutt, T., & Blumenthal, D. K. (1986) *J. Biol. Chem. 264*, 8054.

Dobrowolski, Z., Xu, G.-Q., Chen, W., & Hitchcock-DeGregori, S. E. (1991) *Biochemistry 30*, 7089.

Farrah, C. S., Miyamoto, C. A., Ramos, C. H. I., da Silva, A. C. R., Quaggio, R. B., Fujimori, K., Smillie, L. B., & Reinach, F. C. (1994) *J. Biol. Chem. 269*, 5230.

Finch, J. T., Lutter, L. C., Rhodes, D., Brown, R. S., Rushton, B., Levitt, M., & Klug, A. (1977) *Nature (London) 269*, 29.

Grabarek, Z., Drabikowski, W., Leavis, P. C., Rosenfeld, S. S., & Gergely, J. (1981) *J. Biol. Chem. 256*, 13121.

Heidorn, D. B., & Trewhella, J. (1988) *Biochemistry 27*, 909.

Heidorn, D. B., Seeger, P. A., Rokop, S. E., Blumenthal, D. K., Means, A. R., Crespi, H., & Trewhella, J. (1989) *Biochemistry 28*, 6757.

Herzberg, O., & James, M. N. G. (1985) *J. Biol. Chem. 261*, 2638.

Herzberg, O., Moult, J., & James, M. N. G. (1986) *J. Biol. Chem. 261*, 2638.

Hjelm, R. P., Kneale, G. G., Suau, P., Baldwin, J. P., & Bradbury, E. M. (1977) *Cell 10*, 139.

Ikura, M., Clore, G. M., Gronenborn, A. M., Zhu, G., Klee, C. B., & Bax, A. (1992) *Science 256*, 632.

Kobayashi, T., Tao, T., Gabarek, Z., Gergely, J., & Collins, J. H. (1991) *J. Biol. Chem. 266*, 13746.

Kobayashi, T., Tao, T., Gabarek, Z., Gergely, J., & Collins, J. H. (1994) *J. Biol. Chem. 269*, 5725.

Leavis, P. C., & Gergely, J. (1984) *CRC Crit. Rev. Biochem. 16*, 235.

Leszyk, J., Dumaswala, R., Potter, J. D., Gusev, N. B., Verin, A. D., Tobacman, L. S., & Collins, J. H. (1987) *Biochemistry 26*, 7035.

Leszyk, J., Gabarek, Z., Gergely, J., & Collins, J. H. (1990) *J. Am. Chem. Soc. 29*, 299.

Meador, W. E., Means, A. R., & Quiocho, F. A. (1992) *Science 257*, 1251.

Meador, W. E., Means, A. R., & Quiocho, F. A. (1993) *Science 262*, 1718.

Moore, P. B. (1980) *J. Appl. Crystallogr. 13*, 168.

Ngai, S.-M., & Hodges, R. S. (1992) *J. Biol. Chem. 267*, 15715.

Olah, G. A., Trakhanov, S., Trewhella, J., & Quiocho, F. A. (1993) *J. Biol. Chem. 268*, 16241.

Olah, G. A., Rokop, S. E., Wang, C.-L. A., Blechner, S. L., & Trewhella, J. (1994) *Biochemistry 33*, 8233.

Pardon, J. F., Worcester, D. L., Wooley, J. C., Tatchell, K., Van Holde, K. E., & Richards, B. M. (1975) *Nucleic Acids Res. 2*, 2163.

Pardon, J. F., Worcester, D. L., Wooley, J. C., Cotter, R. I., Lilley, D. M. J., & Richards, B. M. (1977) *Nucleic Acids Res. 4*, 3199.

Potter, J. D., & Gergely, J. (1975) *J. Biol. Chem. 250*, 4628.

Rayment, I., Rypniewski, W. R., Schmidt-Bäse, K., Smith, R., Tomchick, D. R., Benning, M. M., Winkelmann, D. A., Wesenberg, G., & Holden, H. M. (1993) *Science 261*, 50.

Sheng, Z., Francois, J.-M., Hitchcock-DeGregori, S. E., & Potter, J. D. (1991) *J. Biol. Chem. 266*, 5711.

Sundaralingam, M., Bergstrom, R., Strasburg, G., Rao, S. T., Roychowdhury, P., Greaser, M., & Wang, B. C. (1985) *Science 227*, 945.

Syska, H., Wilkinson, J. M., Grand, J. A., & Perry, S. V. (1976) *Biochem. J. 153*, 375.

Talbot, J. A., & Hodges, R. S. (1981) *J. Biol. Chem. 256*, 2798.

Tao, T., Scheiner, C. J., & Lamkin, M. (1986) *Biochemistry 25*, 7633.

Trewhella, J., Blumenthal, D. K., Rokop, S. E., & Seeger, P. A. (1990) *Biochemistry 29*, 9316.

Wilkinson, M., & Grand, R. J. A. (1975) *Biochem. J. 149*, 493.

Wilkinson, M., & Grand, R. J. A. (1978) *Nature 271*, 31.

Xie et al. (1994) *Nature 368*, 306.

Zot, A. S., & Potter, J. D. (1987) *Annu. Rev. Biophys. Biophys. Chem. 16*, 535.